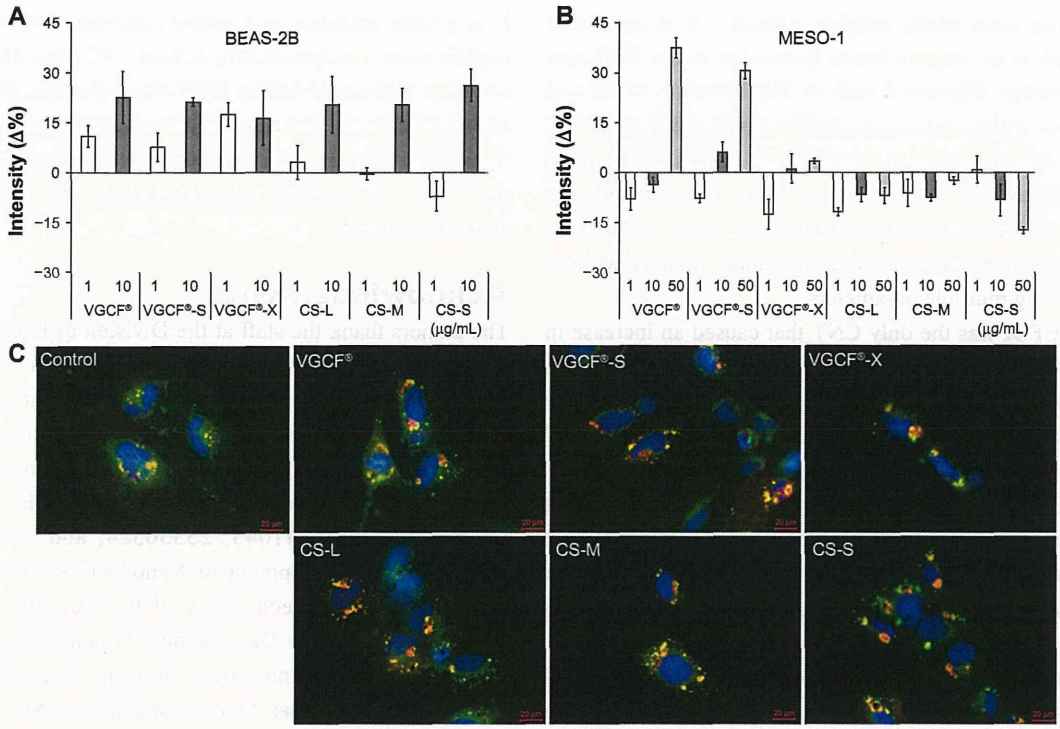

Figure 6 Intracellular acidification upon exposure to CNTs.

Notes: (**A**) BEAS-2B cells were exposed to 1 and 10 μg/mL of MWCNT (VGCF®-X, VGCF®-S, and VGCF®) or CSCNT (CS-L, CS-S, and CS-M) for 24 hours. (**B**) MESO-1 cells were exposed to 1, 10, and 50 μg/mL MWCNT or CSCNT for 24 hours, incubated with an acidotropic probe (LysoSensor™; Life Technologies, Carlsbad, CA, USA), and analyzed by flow cytometry (10,000 cells). The LysoSensor intensity (%) was calculated as follows: ([FL1 channel intensity of cells exposed to CNTs – FL1 channel intensity of untreated cells]/[FL1 channel intensity of cells exposed to DM – FL1 channel intensity of untreated cells]) ×100%. DM is 0.001% gelatin. CNT inhibition intensity (%) was calculated as follows: ([FL1 channel intensity of CNT blank – FL1 channel intensity of untreated cells]/[FL1 channel intensity of DM blank – FL1 channel intensity of untreated cells]) ×100%. The intensity change was determined as follows: intensity (Δ%) = LysoSensor intensity (%) – CNT inhibition intensity (%). Data are expressed as mean ± standard error (n=4). (**C**) BEAS-2B cells were exposed to 10 μg/mL MWCNT (VGCF, VGCF-S, and VGCF-X) or CSCNT (CS-L, CS-M, and CS-S) for 24 hours and visualized by staining with LysoSensor dye (green), CellLight® Lysosomes-RFP (red [Life Technologies]), and bisbenzimide H33342 fluorochrome trihydrochloride (blue [Nacalai Tesque, Kyoto, Japan]) for nuclei. Scale bar =20 μm. MWCNTs were provided by Showa Denko KK (Tokyo, Japan); CSCNTs were provided by GSI Creos (Tokyo, Japan).

Abbreviations: CNT, carbon nanotube; CSCNT, cup-stacked carbon nanotube; DM, dispersant medium; MWCNT, multi-walled carbon nanotube; CS-L, CSCNT of length 20–80 μm; CS-S, CSCNT of length 0.5–20 μm; CS-M, CSCNT of intermediate length; VGCF, vapor grown carbon fibers.

epithelial cells, were shown to take up MWCNTs, whereas cytotoxicity was comparable to what was observed in BEAS-2B cells or MESO-1 cells in the present study.[8] The discordance between those results and ours may be the difference in internalization time. The previous study evaluated CNT uptake after 3 hours of MWCNT exposure, and evaluated cytotoxicity on the fourth day. Cellular uptake is dependent on time and cell type, and therefore a 3-hour exposure may be too short to evaluate the full extent of endocytosis.[14,32] In contrast, CSCNTs were not toxic to MESO-1 cells; however, in BEAS-2B cells, toxicity was also dependent on size (in this case, length), with toxicity values of CS-L ≥ CS-M > CS-S (Figure 1). These results are consistent with reports that have demonstrated a positive association between CNT length and cytotoxicity.[5,40,41] Although the cytotoxicity of CSCNTs of a given diameter was comparable between cell lines, VGCF-X, which is shorter than VGCF-S, was more toxic to BEAS-2B cells. VGCF-X had the shortest length and smallest diameter among the CNTs tested in this study. However, VGCF-X agglomerates had the largest diameter, and, as such, were not taken up by BEAS-2B cells, nor did they fully penetrate the cell membrane (Figures 3d and 4f). We previously reported that the volume of BEAS-2B cells is less than half of that of MESO-1 cells.[32] Smaller cells may be more susceptible to cytotoxicity because of incomplete endocytosis of a CNT aggregate. This is supported by the observation that LDH activity was highest in BEAS-2B cells exposed to VGCF-X. Moreover, the fact that CS-L and CS-M induced cytotoxicity to a comparable or lesser degree than VGCF despite their greater lengths could indicate that cytotoxicity is related to CNT rigidity, which has been previously suggested.[8] Although CSCNTs were similar in diameter to VGCF-S, they have greater flexibility, which predisposes them to

becoming more easily tangled. Indeed, CS-M and CS-S appeared to be tangled inside lysosomes in the TEM and LSM images (Figures 3 and 4). Furthermore, CS-L and VGCF-S aggregates have similar shape (Figure 3) and comparable cytotoxicity values. These results demonstrate that CNT toxicity is a function not only of tube length and rigidity, but also cell and aggregate sizes, and it is therefore imprudent to make generalizations about toxicity without considering multiple parameters.

VGCF-X was the only CNT that caused an increase in total ROS (Figure 5). This indicates that CNTs are not, in general, inducers of oxidative stress in cells. It was recently shown that CNTs can act as OH radical scavengers.[12,42–44] However, VGCF-X has a higher iron content than VGCF or VGCF-S, since it was not subjected to iron removal heat treatment, and iron is a potential source of ROS. Nonetheless, stimulation of intracellular total ROS production did not directly contribute to cytotoxicity in MESO-1 cells.

We speculated that damage to the lysosome could be the cause of cytotoxicity. In fact, non-aggregated VGCF and VGCF-S penetrated the lysosomal membrane, as seen in the TEM images (Figure 4Ac and e and 4Bc and e). Despite this, the signal intensity of injured, fluorescently labeled lysosomes remained unchanged. We recently reported that highly purified MWCNTs induced the expression of the autophagic marker light chain 3B, and 3-MA – a widely used inhibitor of autophagosome formation – reduced MWCNT-induced cytotoxicity in BEAS-2B cells.[45] This was further validated by the present observation that cells exposed to CNTs showed increased acidification as a result of autophagy.[46] Intracellular acidification was observed in MESO-1 cells only when exposed to VGCF and VGCF-S at a concentration of 50 μg/mL, whereas VGCF-X used at the same concentration did not have this effect while inducing a comparable degree of cytotoxicity as VGCF-S. This study was unable to clarify how autophagy was triggered. However, since acidification was unlikely to occur in lysosomes that had endocytosed CS-S, as in the case of carbon black (reported in our previous study),[33] it is probable that the shape and size of CNTs are involved in promoting autophagy.

Conclusion

The cellular response to different types of CNTs of various dimensions was evaluated. CSCNTs, with their larger surface area, are more useful for functionalization, and the length can be adjusted by ball milling.[34,47] CSCNTs were also more biocompatible than MWCNTs, and therefore have greater potential as a nanobiomaterial, despite being slightly toxic. The cytotoxicity of both CNTs was dependent on many factors, including CNT shape (length, diameter, and aggregation), but also varied according to cell type. Therefore, it is necessary to confirm biocompatibility in each target cell type when considering the use of CNTs as a nanobiomaterial.

Acknowledgments

The authors thank the staff at the Division of Instrumental Analysis in the Research Center for Human and Environmental Sciences of Shinshu University for their assistance. This research was supported by the Regional Innovation Cluster Program (second stage) of the Ministry of Education, Culture, Sports, Science, and Technology of Japan; JSPS KAKENHI grant numbers 24241045, 25350524, and 25462365; Research and Development of Nanodevices for Practical Utilization of Nanotechnology of the New Energy and Industrial Technology Development Organization, Japan; the Japan Regional Innovation Strategy Program by the Excellence of the Japan Science and Technology Agency; the Adaptable and Seamless Technology Transfer Program through Target-driven R&D; and the Hospital-Company Collaboration Support Project for Developing/Improving Problem-Solving-Type Medical Equipment by the Ministry of Economy, Trade, and Industry, Japan.

Disclosure

The authors report no conflicts of interest in this work.

References

1. Saito N, Usui Y, Aoki K, et al. Carbon nanotubes: biomaterial applications. *Chem Soc Rev*. 2009;38(7):1897–1903.
2. Li X, Fan Y, Watari F. Current investigations into carbon nanotubes for biomedical application. *Biomed Mater*. 2010;5(2):22001.
3. Adams D, Williams DF. The response of bone to carbon – carbon composites. *Biomaterials*. 1984;5(2):59–64.
4. Bokros JC. Carbon biomedical devices. *Carbon*. 1977;15(6):353–371.
5. Poland CA, Duffin R, Kinloch I, et al. Carbon nanotubes introduced into the abdominal cavity of mice show asbestos-like pathogenicity in a pilot study. *Nat Nanotechnol*. 2008;3(7):423–428.
6. Takagi A, Hirose A, Nishimura T, et al. Induction of mesothelioma in p53± mouse by intraperitoneal application of multi-wall carbon nanotube. *J Toxicol Sci*. 2008;33(1):105–116.
7. Sakamoto Y, Nakae D, Fukumori N, et al. Induction of mesothelioma by a single intrascrotal administration of multi-wall carbon nanotube in intact male Fischer 344 rats. *J Toxicol Sci*. 2009;34(1):65–76.
8. Nagai H, Okazaki Y, Chew SH, et al. Diameter and rigidity of multiwalled carbon nanotubes are critical factors in mesothelial injury and carcinogenesis. *Proc Natl Acad Sci U S A*. 011;108(49):E1330–E1338.
9. Kobayashi N, Naya M, Ema M, et al. Biological response and morphological assessment of individually dispersed multi-wall carbon nanotubes in the lung after intratracheal instillation in rats. *Toxicology*. 2010;276(3):143–153.

10. Ellinger-Ziegelbauer H, Pauluhn J. Pulmonary toxicity of multi-walled carbon nanotubes (Baytubes) relative to alpha-quartz following a single 6h inhalation exposure of rats and a 3 months post-exposure period. *Toxicology*. 2009;266(1–3):16–29.
11. Ma-Hock L, Treumann S, Strauss V, et al. Inhalation toxicity of multiwall carbon nanotubes in rats exposed for 3 months. *Toxicol Sci*. 2009;112(2):468–481.
12. Porter DW, Hubbs AF, Mercer RR, et al. Mouse pulmonary dose- and time course-responses induced by exposure to multi-walled carbon nanotubes. *Toxicology*. 2010;269(2–3):136–147.
13. Muller J, Delos M, Panin N, Rabolli V, Huaux F, Lison D. Absence of carcinogenic response to multiwall carbon nanotubes in a 2-year bioassay in the peritoneal cavity of the rat. *Toxicol Sci*. 2009;110(2): 442–448.
14. Hirano S, Fujitani Y, Furuyama A, Kanno S. Uptake and cytotoxic effects of multi-walled carbon nanotubes in human bronchial epithelial cells. *Toxicol Appl Pharmacol*. 2010;249(1):8–15.
15. Tabet L, Bussy C, Amara N, et al. Adverse effects of industrial multiwalled carbon nanotubes on human pulmonary cells. *J Toxicol Environ Health A*. 2009;72(2):60–73.
16. Jacobsen NR, Pojana G, White P, et al. Genotoxicity, cytotoxicity, and reactive oxygen species induced by single-walled carbon nanotubes and C(60) fullerenes in the FE1-Mutatrade markMouse lung epithelial cells. *Environ Mol Mutagen*. 2008;49(6):476–487.
17. Monteiro-Riviere NA, Nemanich RJ, Inman AO, Wang YY, Riviere JE. Multi-walled carbon nanotube interactions with human epidermal keratinocytes. *Toxicol Lett*. 2005;155(3):377–384.
18. Yang H, Liu C, Yang D, Zhang H, Xi Z. Comparative study of cytotoxicity, oxidative stress and genotoxicity induced by four typical nanomaterials: the role of particle size, shape and composition. *J Appl Toxicol*. 2009;29(1):69–78.
19. Davoren M, Herzog E, Casey A, et al. In vitro toxicity evaluation of single walled carbon nanotubes on human A549 lung cells. *Toxicol In Vitro*. 2007;21(3):438–448.
20. De Nicola M, Gattia DM, Bellucci S, et al. Effect of different carbon nanotubes on cell viability and proliferation. *J Phys Condens Matter*. 2007;19(39):395013–395019.
21. Magrez A, Kasas S, Salicio V, et al. Cellular toxicity of carbon-based nanomaterials. *Nano Lett*. 2006;6(6):1121–1125.
22. Wick P, Manser P, Limbach LK, et al. The degree and kind of agglomeration affect carbon nanotube cytotoxicity. *Toxicol Lett*. 2007;168(2): 121–131.
23. Coccini T, Roda E, Sarigiannis DA, et al. Effects of water-soluble functionalized multi-walled carbon nanotubes examined by different cytotoxicity methods in human astrocyte D384 and lung A549 cells. *Toxicology*. 2010;269(1):41–53.
24. Muller J, Huaux F, Fonseca A, et al. Structural defects play a major role in the acute lung toxicity of multiwall carbon nanotubes: toxicological aspects. *Chem Res Toxicol*. 2008;21(9):1698–1705.
25. Sato Y, Yokoyama A, Shibata K, et al. Influence of length on cytotoxicity of multi-walled carbon nanotubes against human acute monocytic leukemia cell line THP-1 in vitro and subcutaneous tissue of rats in vivo. *Mol Biosyst*. 2005;1(2):176–182.
26. Bottini M, Bruckner S, Nika K, et al. Multi-walled carbon nanotubes induce T lymphocyte apoptosis. *Toxicol Lett*. 2006;160(2):121–126.
27. Kolosnjaj-Tabi J, Hartman KB, Boudjemaa S, et al. In vivo behavior of large doses of ultrashort and full-length single-walled carbon nanotubes after oral and intraperitoneal administration to Swiss mice. *ACS Nano*. 2010;4(3):1481–1492.
28. Pulskamp K, Diabaté S, Krug HF. Carbon nanotubes show no sign of acute toxicity but induce intracellular reactive oxygen species in dependence on contaminants. *Toxicol Lett*. 2007;168(1):58–74.
29. Kagan VE, Tyurina YY, Tyurin VA, et al. Direct and indirect effects of single walled carbon nanotubes on RAW 264.7 macrophages: role of iron. *Toxicol Lett*. 2006;165(1):88–100.
30. Ge C, Du J, Zhao L, et al. Binding of blood proteins to carbon nanotubes reduces cytotoxicity. *Proc Natl Acad Sci U S A*. 2011;108(41): 16968–16973.
31. Kim JS, Song KS, Lee JH, Yu IJ. Evaluation of biocompatible dispersants for carbon nanotube toxicity tests. *Arch Toxicol*. 2011;85(12): 1499–1508.
32. Haniu H, Saito N, Matsuda Y, et al. Effect of dispersants of multi-walled carbon nanotubes on cellular uptake and biological responses. *Int J Nanomedicine*. 2011;6:3295–3307.
33. Haniu H, Saito N, Matsuda Y, et al. Elucidation mechanism of different biological responses to multi-walled carbon nanotubes using four cell lines. *Int J Nanomedicine*. 2011;6:3487–3497.
34. Kim YA, Hayashi T, Fukai Y, Endo M, Yanagisawa T, Dresselhaus MS. Effect of ball milling on morphology of cup-stacked carbon nanotubes. *Chem Phys Lett*. 2002;355(3–4):279–284.
35. Usami N, Fukui T, Kondo M, et al. Establishment and characterization of four malignant pleural mesothelioma cell lines from Japanese patients. *Cancer Sci*. 2006;97(5):387–394.
36. Ma X, Wu Y, Jin S, et al. Gold nanoparticles induce autophagosome accumulation through size-dependent nanoparticle uptake and lysosome impairment. *ACS Nano*. 2011;5(11):8629–8639.
37. Allen BL, Kichambare PD, Gou P, et al. Biodegradation of single-walled carbon nanotubes through enzymatic catalysis. *Nano Lett*. 2008;8(11):3899–3903.
38. Kagan VE, Konduru NV, Feng W, et al. Carbon nanotubes degraded by neutrophil myeloperoxidase induce less pulmonary inflammation. *Nat Nanotechnol*. 2010;5(5):354–359.
39. Sato Y, Yokoyama A, Nodasaka Y, et al. Long-term biopersistence of tangled oxidized carbon nanotubes inside and outside macrophages in rat subcutaneous tissue. *Sci Rep*. 2013;3:2516.
40. Murphy FA, Schinwald A, Poland CA, Donaldson K. The mechanism of pleural inflammation by long carbon nanotubes: interaction of long fibres with macrophages stimulates them to amplify pro-inflammatory responses in mesothelial cells. *Part Fibre Toxicol*. 2012;9:8.
41. Liu D, Wang L, Wang Z, Cuschieri A. Different cellular response mechanisms contribute to the length-dependent cytotoxicity of multi-walled carbon nanotubes. *Nanoscale Res Lett*. 2012;7(1):361.
42. Fenoglio I, Aldieri E, Gazzano E, et al. Thickness of multiwalled carbon nanotubes affects their lung toxicity. *Chem Res Toxicol*. 2012;25(1): 74–82.
43. Fenoglio I, Tomatis M, Lison D, et al. Reactivity of carbon nanotubes: free radical generation or scavenging activity? *Free Radic Biol Med*. 2006;40(7):1227–1233.
44. Fenoglio I, Greco G, Tomatis M, et al. Structural defects play a major role in the acute lung toxicity of multiwall carbon nanotubes: physicochemical aspects. *Chem Res Toxicol*. 2008;21(9): 1690–1697.
45. Tsukahara T, Matsuda Y, Usui Y, Haniu H. Highly purified, multi-wall carbon nanotubes induce light-chain 3B expression in human lung cells. *Biochem Biophys Res Commun*. 2013;440(2):348–353.
46. Klionsky DJ, Emr SD. Autophagy as a regulated pathway of cellular degradation. *Science*. 2000;290(5497):1717–1721.
47. Endo M, Kim YA, Ezaka M, et al. Selective and efficient impregnation of metal nanoparticles on cup-stacked-type carbon nanofibers. *Nano Lett*. 2003;3:723–726.

Journal of the Ceramic Society of Japan 122 [4] 292-299 2014 Technical report

Influence of CNF content on microstructure and fracture toughness of CNF/alumina composites

Naoki UEDA, Tomohiko YAMAKAMI, Tomohiro YAMAGUCHI, Yuki USUI,* Kaoru AOKI,* Morinobu ENDO, Naoto SAITO and Seiichi TARUTA†**

Faculty of Engineering, Shinshu University, 4–17–1 Wakasato, Nagano 380–8553, Japan
***Shinshu University School of Medicine, 3–1–1 Asahi, Matsumoto, Nagano 390–8621, Japan**
****Department of Applied Physical Therapy, Shinshu University School of Health Sciences, 3–1–1 Asahi, Matsumoto, Nagano 390–8621, Japan**

Dense 0.4–5.0 wt % carbon nanofiber (CNF)/alumina composites were fabricated by plasma activated sintering. The microstructure—particularly the CNFs distribution—of composites containing different amounts of CNFs was observed in detail, and the influence of the additive amounts of CNF on the microstructure and the fracture toughness of the composites were investigated. The ratio of CNFs distributed individually in the composites decreased with an increase in the addition of CNFs, and the other CNFs formed bundles; notably three-quarters of the CNFs formed bundles in the 5.0 wt % CNF/alumina composite. The alumina grain size distribution of the composites became narrower to smaller grain size side and the average alumina grain size of the composites decreased with an increase in the addition of CNFs from 0.4 to 1.6 wt %. However, the average alumina grain size of the composites did not vary greatly with an increase in the addition of CNFs from 1.6 to 5.0 wt %, because the CNF bundles formed in the 2.5 and 5.0 wt % CNF/alumina composites lowered the grain growth retardation effect of the CNFs. The 1.6 wt % CNF/alumina composite exhibited the highest fracture toughness, because three-fifths of the CNFs distributed individually and uniformly in alumina grain boundaries.

Key-words : Alumina, Carbon nanofibers, Composite, Fracture toughness, Microstructure

[Received August 23, 2013; Accepted February 1, 2014]

1. Introduction

Carbon nanotubes (CNTs) have incredible mechanical properties and a high aspect ratio,[1)–8)] so it seems that CNTs are superior reinforcement fibers for the improvement of the mechanical properties of ceramic materials. With that aim in mind for alumina ceramics, we have combined the high-dispersion-treated carbon nanofibers (CNFs), which are a type of multi-walled CNTs, with alumina.[9)] In the study, we found that the fracture toughness of the CNF/alumina composites increased with a decrease in the average alumina grain size of the composites, regardless of CNF content in the range of 0.4–2.5 wt %.[9)] In these composites, CNFs were observed bending along alumina grain boundaries. The dependence of the fracture toughness of the composites on the average alumina grain size could be explained by the bridging and/or pull-out of the bended CNFs. That is, the number of bendings per CNF increased as the average alumina grain size of the composites decreased. As the number of bendings increased, the resistance for bridging and/or pull-out of the CNFs increased. Consequently, the fracture toughness of the composites increased with a decrease in the average alumina grain size. On the other hand, the CNFs were gathered at the same sites in the grain boundaries and formed bundles through the grain growth of alumina during sintering, especially in the composites containing larger amounts of CNFs. By forming CNF bundles, the number of CNFs giving rise to the essential effect for bridging and/or pull-out was reduced, and the resistance for bridging and/or pull-out of CNFs in the composites did not always increase with an increase in the additive amount of CNFs. Consequently, the fracture toughness of the composite was not greatly influenced by the additive amount of CNFs.

Some reports[10)–16)] on CNT/alumina composites have shown that the fracture toughness of composites does not always greatly increase with an increase in the additive amount of CNTs. For example, Yamamoto et al.[12)] reported that the fracture toughness of the CNT/alumina composites decreased with increasing MWCNTs content from 0–10 mass % because of the presence of CNT aggregates. Hirota et al.[14)] reported that the fracture toughness of the 3–5 vol % CNF/alumina composites showed a slight increase compared to that of monolithic alumina. Maensiri et al.[15)] reported that the fracture toughness of the CNF/alumina composites increased with a slight dependency on the additive amount of CNFs, and a 13% increase in fracture toughness compared to monolithic alumina was obtained in the 2.5 vol % CNF/alumina composite.

In order to achieve a further improvement in the fracture toughness of CNT/alumina composites by the addition of a larger amount of CNTs, the CNTs should distribute individually and uniformly in the composites. However, the influence of CNTs distribution on microstructure development and the mechanical properties of the CNT/alumina composites containing a different amount of CNTs has not yet been reported in detail.

In our first paper[9)] on the CNF/alumina composites, we reported as mentioned above that the 0.4–2.5 wt % CNF/alumina composites were fabricated using the high-dispersion-treated CNFs and the influence of the addition of the CNFs on the densification, microstructure development and mechanical properties of the composites were investigated. In our second paper,[17)]

† Corresponding author: S. Taruta; E-mail: staruta@shinshu-u.ac.jp

DOI http://dx.doi.org/10.2109/jcersj2.122.292

we reported that the 0.4 wt% CNF/alumina composites were fabricated using CNFs acid-treated for 0.5, 1 and 5 h. The CNFs acid-treated for 0.5 h dispersed more uniformly in the composite than the high-dispersion-treated CNFs and the composite containing the CNFs acid-treated for 0.5 h had a smaller average alumina grain size and higher fracture toughness. Now, in this study, the CNFs acid-treated for 0.5 h were mixed with alumina and the 0.4–5.0 wt% CNFs/alumina composites were fabricated by plasma activated sintering (PAS). The microstructures—particularly the CNFs distributions—of the composites containing different amount of CNFs were qualitatively estimated by observing the backscattered electron (BSE) images of polished surfaces of these composites under accelerating voltage of 1 kV and were quantitatively estimated by observing the scanning electron microscopic images of polished and chemically etched surfaces of these composites. Such qualitative and quantitative estimations have neither been tried in our previous studies[9),17)] nor in other studies on CNF/ceramics composites and were carried out for the first time by us in this study. The influence of the additive amount of the CNFs on CNF distribution, alumina grain size distribution and fracture toughness of the composites fabricated by PAS were investigated.

2. Experimental procedure

2.1 Preparation of the acid-treated CNFs and the composites

CNFs (VGCF-S; diameter: 100 nm, length: 10–20 μm, Showa Denko, Japan) were acid-treated for 0.5 h using an acid mixture (conc. H_2SO_4: conc. HNO_3 = 3:1 v/v) under application of ultrasonic agitation in order to prepare the hydrophilic CNFs and improve interfacial compatibility between CNFs and the alumina grain. Raman spectra of the CNFs showed that defects were induced on them by the acid-treatment for 0.5 h.[17)]

The acid-treated CNFs were ultrasonically dispersed in ethanol solution dissolving a small amount of polyvinylbutyral (PVB) as a dispersant. The CNF-ethanol suspensions were quietly kept for 3 days to allow the remaining bundles or agglomerates of CNF sediment in the bottom layer of the suspensions. Then, the upper layer of the suspensions was elutriated to obtain well dispersed CNF suspensions. These were mixed with high-purity alumina powder (TM-DAR; purity: 99.99%; average particle size: 0.1 μm; Taimei Chemicals, Japan) by ball-milling for 24 h. The obtained slurries were dried and then passed through a 100-mesh sieve. In this way, the powder mixtures containing 0.4–5.0 wt% CNFs were prepared.

The powder mixtures were consolidated by plasma activated sintering (Ed-PAS, ELENIX) at 1300–1525°C for 80 s in a vacuum. They were put under an uniaxial pressure of 50 MPa during PAS, except for the powder mixture containing 1.6 wt% CNFs sintered by PAS at 1375°C, which was put under an uniaxial pressure of 40 MPa during PAS. The heating rate of PAS was 300°C/min.

2.2 Estimation of composites

The bulk densities of the composites were measured using the Archimedes method. The relative densities were calculated using the bulk densities of the composites and the theoretical densities of alumina (3.987 g/cm^3) and VGCF-S (2.0 g/cm^3). The microstructures of the composites were observed using a scanning electron microscope (SEM, S-4100 or SU-8000, Hitachi).

The fracture toughness was measured using the Vickers indentation tester (VMT-7, MATSUZAWA). An 196 N load was applied on the polished surface for 10 s. For the composites which crack tipping were observed, a lower indentation load (98 N) was applied on the polished surface. The crack-to-indent ratios (c/a) were larger than 2.5 in every indentation, where c is the half-length of the surface radial crack and a is the half-diagonal length of the Vickers indent. This means cracks propagated in the composites were median cracks.[18)–20)] So the fracture toughness was calculated by Miyoshi's formula.[21)]

The alumina grain sizes of the composites were measured using the line-intercept method.[22)] The measured individual grain size was the maximum length of the grain, which is described as tangent diameter,[23),24)] in the specified direction. The average alumina grain size was determined from the sizes of more than 200 grains. The details for preparation of the specimen were shown in our previous reports.[9),17)]

3. Results and discussions

3.1 Densification

The relative densities of the 0.4–5.0 wt% CNF/alumina composites and monolithic alumina ceramic are shown in **Fig. 1**. Regardless of the additive amount of CNFs, the relative densities of the composites sintered by PAS at 1375°C for 80 s were more than 99%. In addition, the 0.4–1.6 wt% CNF/alumina composites sintered by PAS at 1300 and 1450°C, and the 2.5 and 5.0 wt% CNF/alumina composites sintered by PAS at 1450 and 1525°C were densified to a relative density of more than 99%. On the other hand, the relative densities of the composites sintered in vacuum at 1350°C for 2 h decreased drastically with an increase in the additive amount of CNFs, as shown in Fig. 1. Similar results were obtained for the composites sintered in vacuum at 1450°C. Though the holding time of PAS was 100 times shorter than that of vacuum sintering, even the composites containing 5.0 wt% CNFs were densified to near the full density by PAS. These results indicate that the densification rate of the composites was accelerated by the unique sintering process of PAS.

3.2 Microstructures

SEM images of the chemically etched surfaces of the 0.4–5.0 wt% CNF/alumina composites sintered by PAS at 1375°C for 80 s are shown in **Fig. 2**. The chemical etching for the composites of which the surfaces were polished to a mirror finish was

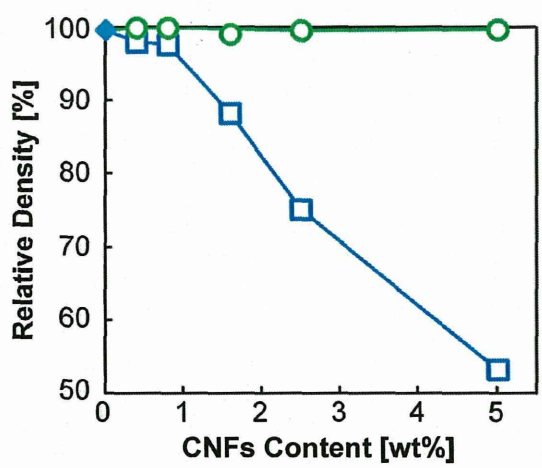

Fig. 1. Relative densities of (○) the 0.4–5.0 wt% CNF/alumina composites sintered by PAS at 1375°C for 80 s, (□) the composites sintered in vacuum at 1350°C for 2 h and (◆) monolithic alumina sintered in air at 1300°C for 2 h and then treated by HIP.

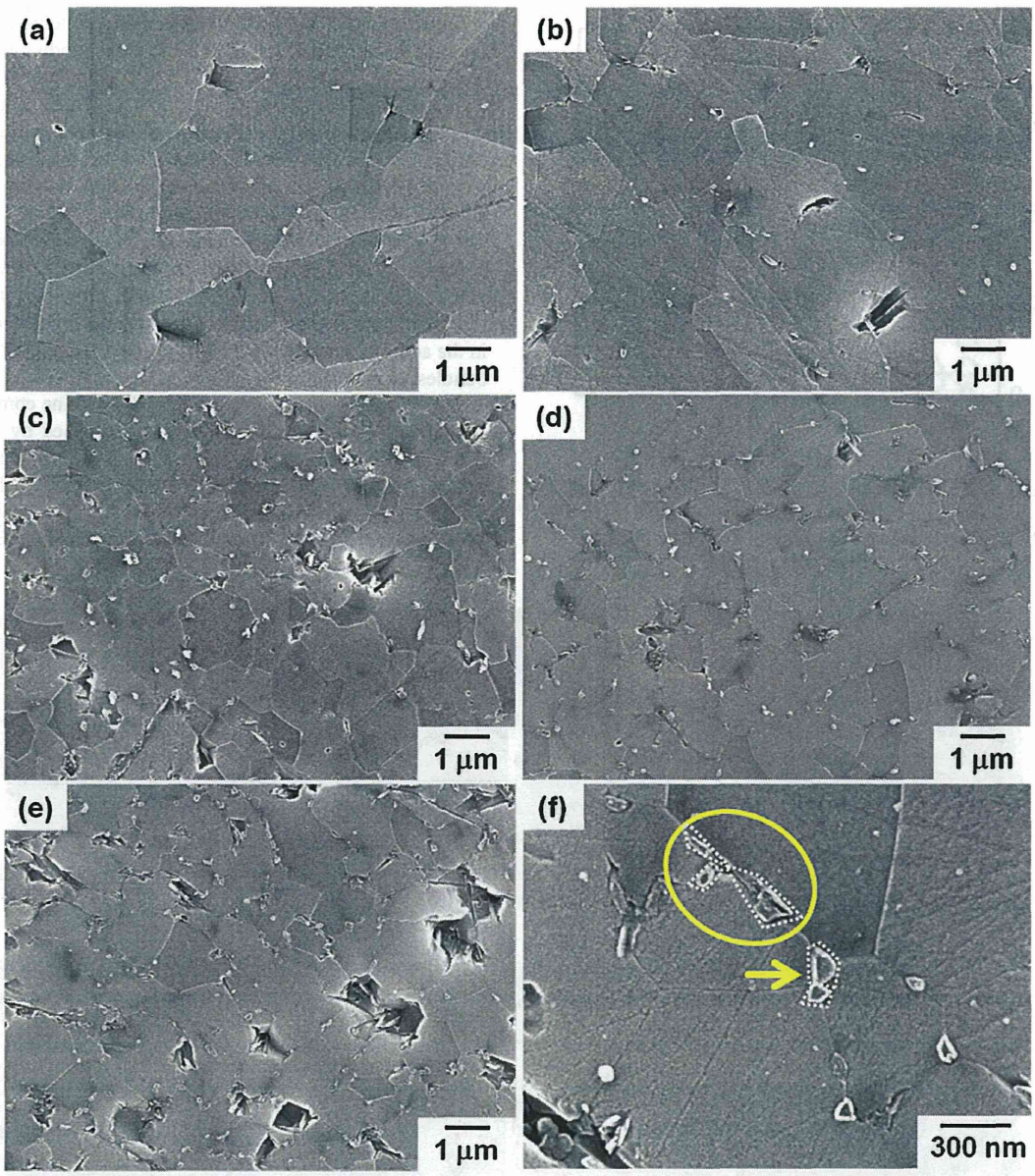

Fig. 2. SEM images of chemically etched surfaces of the (a) 0.4, (b) 0.8, (c) 1.6, (d) 2.5 and (e,f) 5.0 wt% CNFs/alumina composites sintered by PAS at 1375°C for 80 s. The circle and arrow in (f) indicate bundles consisting of three and two CNFs, respectively.

carried out in conc. H_3PO_4 at 140°C for 0.5–1 h. By this etching, not only alumina grain boundaries but also CNFs appeared. The alumina grain sizes became smaller as the additive amount of CNFs increased from 0.4 to 1.6 wt%. However, no such obvious difference in alumina grain sizes was observed in the 1.6–5.0 wt% CNF/alumina composites. Agglomerates of CNFs were not observed in the 0.4–2.5 wt% CNF/alumina composites, but a few agglomerates 5–10 μm in size were observed in the 5.0 wt% CNF/alumina composites. As indicated by an arrow and a circle in Fig. 2(f), two or three CNFs were gathered at the same site in the composites, namely at the grain boundary, which shows that these CNFs formed bundles. In the 0.4 and 0.8 wt% CNF/alumina composites sintered at 1300–1450°C, some CNFs were observed in the alumina grains. Then, the number of CNFs distributed in the alumina grains and at the alumina grain boundaries was counted using SEM photographs of the chemically etched surface of the composites, and the ratio for each composite was determined. The total number of CNFs was at least 370. As the results, in the 0.4 and 0.8 wt% CNF/alumina composites sintered at 1375°C, 17 and 11% of the CNFs entered alumina grains, respectively, while in the 1.6, 2.5 and 5.0 wt% CNF/alumina composites sintered at 1375°C, only 4, 3 and 2% of the CNFs entered alumina grains, respectively. In addition, in the 0.4 wt% CNFs/alumina composite sintered at 1300 and 1450°C, 14 and 20% CNFs entered alumina grains, respectively.

The frequency of solo CNFs and CNF bundles distributed in the 0.4–5.0 wt% CNF/alumina composites sintered at 1375°C for 80 s are shown in **Fig. 3**. The number of solo CNFs and CNF bundles consisting of two, three and more than four CNFs was counted using SEM photographs of the chemically etched surface

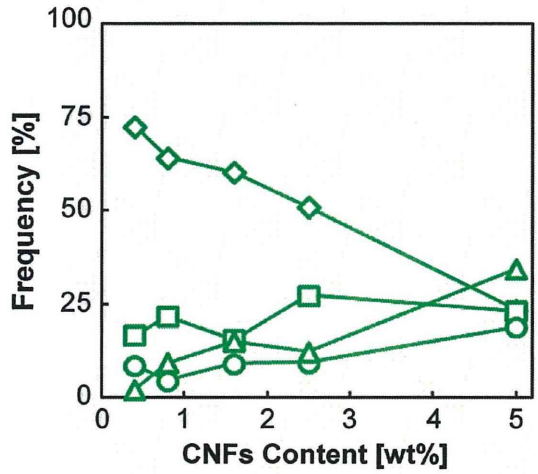

Fig. 3. Frequency of (◇) solo CNF and CNF bundles consisting of (□) two, (○) three and (△) more than four CNFs distributed in the 0.4–5.0 wt% CNF/alumina composites sintered by PAS at 1375°C for 80 s.

of the composites, and the frequencies were determined from the ratios of the number of solo CNFs and CNF bundles consisting of two, three and more than four CNFs to the total number of CNFs. As the results, the frequencies of solo CNFs distributed in the 0.4, 0.8, 1.6, 2.5 and 5.0 wt% CNF/alumina composites were 73, 64, 60, 51 and 24%, respectively. This means that more than three-fifths the number of CNFs were distributed individually in the 0.4–1.6 wt% CNF/alumina composites, half the number of CNFs were distributed individually in the 2.5 wt% CNF/alumina composite, and only a quarter the number of CNFs was individually distributed in the 5.0 wt% CNF/alumina composite. In this way, the frequency of solo CNFs decreased with an increase in the additive amount of CNFs; in reverse, the frequency of CNF bundles increased.

BSE images of the 0.4–5.0 wt% CNF/alumina composites are shown in **Fig. 4**. The composites were polished by ion-milling and were observed using an electron beam under an accelerating voltage of 1 kV without coating of the conductive films. Each alumina grain was confirmed by the channeling contrast of the backscattered electrons. Though the dark areas in the BSE images

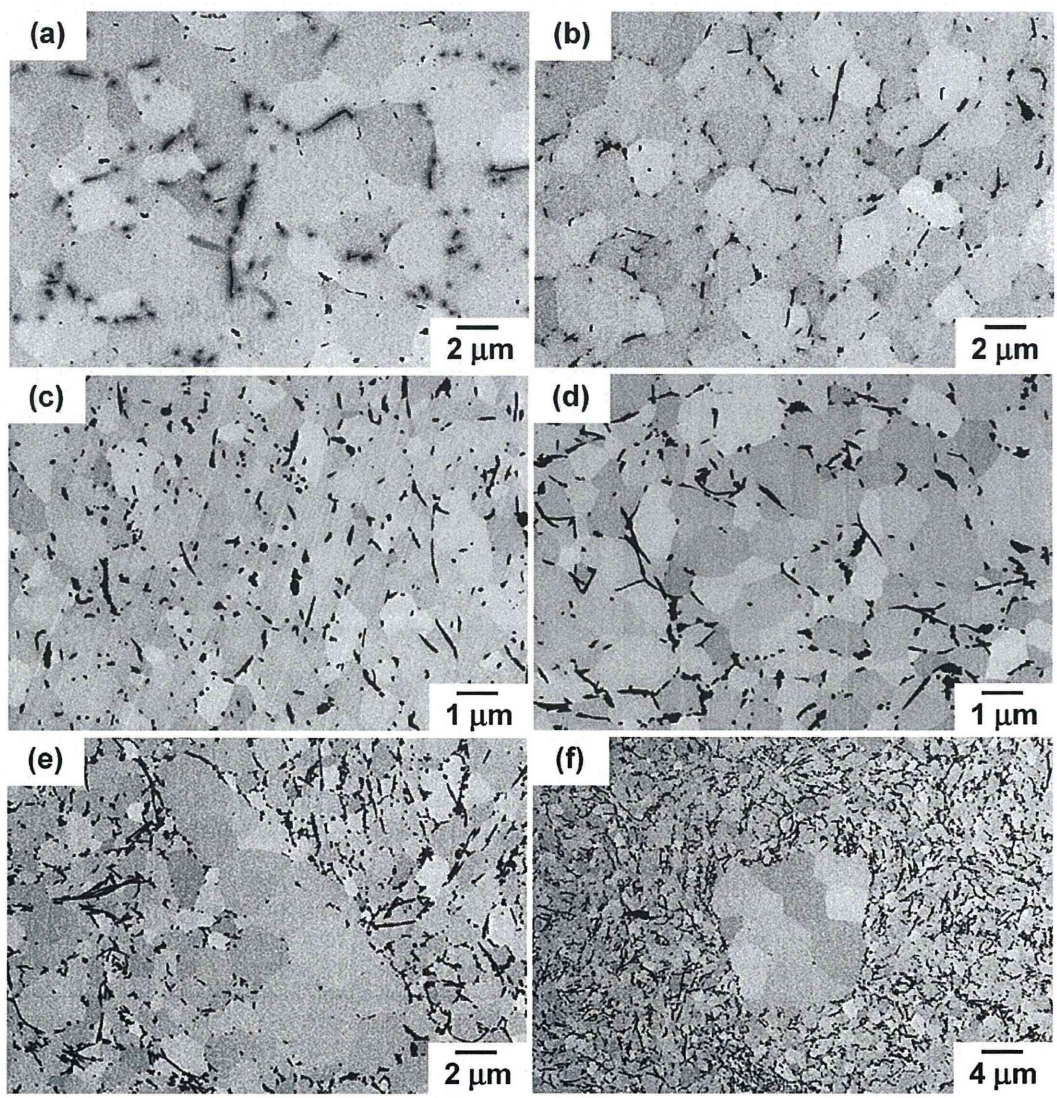

Fig. 4. SEM images of ion-milled surface of the (a) 0.4, (b) 0.8, (c) 1.6, (d) 2.5 and (e,f) 5.0 wt% CNF/alumina composites sintered by PAS at 1375°C for 80 s.

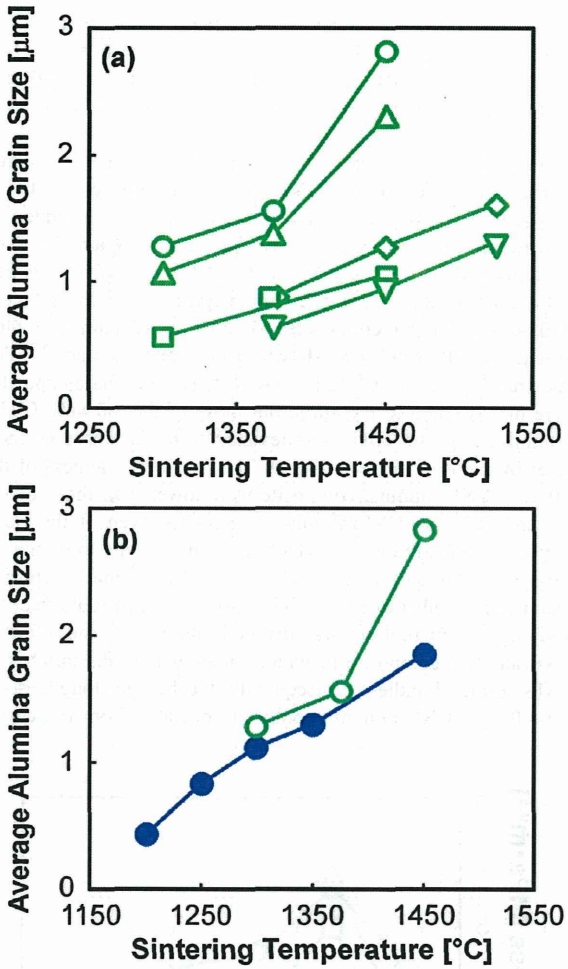

Fig. 5. (a) Average alumina grain sizes of the (○) 0.4, (△) 0.8, (□) 1.6, (◇) 2.5 and (▽) 5.0 wt% CNF/alumina composites sintered by PAS at various temperatures for 80 s. (b) Average alumina grain size of the 0.4 wt% CNF/alumina composites (○) sintered by PAS at various temperatures for 80 s and (●) sintered in vacuum at various temperatures for 2 h and then treated by HIP.

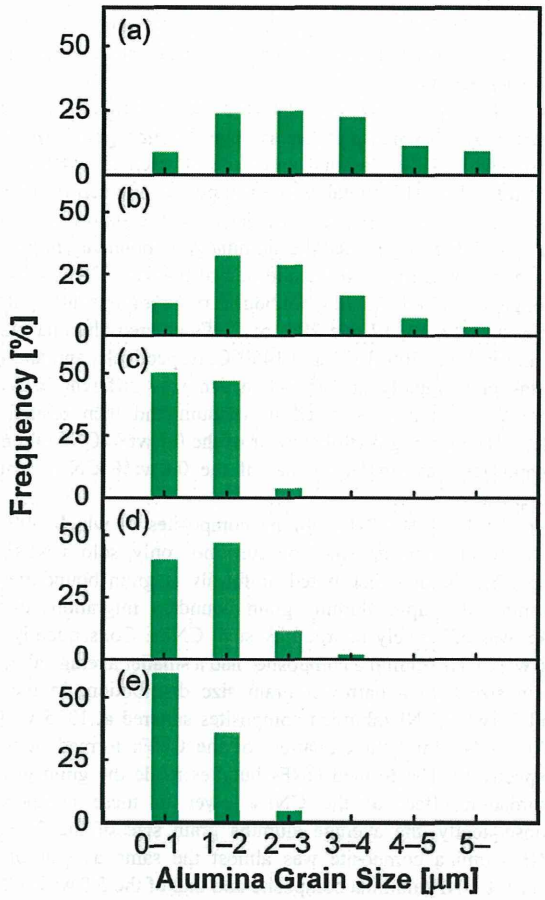

Fig. 6. Alumina grain size distributions of the (a) 0.4, (b) 0.8, (c) 1.6, (d) 2.5 and (e) 5.0 wt% CNF/alumina composites sintered by PAS at 1450°C for 80 s.

of the CNF/alumina composites show either pore or CNF, most dark areas were CNFs because these composites contained few pores. In the 0.4–1.6 wt% CNF/alumina composites, uniform dispersed dot-like and line-like dark areas were observed and a lot of them were around 100 nm in diameter and width, which corresponded to the diameter of the CNF. This resulted from the individual and uniform distribution of more than three-fifths of the CNFs in the composites. On the other side, there were two kinds of region in the 2.5 and 5.0 wt% CNF/alumina composites. One was a region where only a few CNFs were distributed and the other was a region where many CNFs were distributed. In the regions where a few CNFs were distributed, many dark areas were dot-like with sizes of around 100 nm. Such regions in the 5.0 wt% CNF/alumina composite appeared clearly and were much wider than those in the 2.5 wt% CNF/alumina composite. And alumina grains in such regions grew much larger than those in the other regions, especially, it was remarkable in the 5.0 wt% CNF/alumina composite. In the regions where many CNFs were distributed, many dot-like and line-like dark areas were larger than 100 nm, which means that they were CNF bundles. The formation of such CNF bundles and the existence of these two regions suggest that the 2.5 and 5.0 wt% CNFs could not be uniformly mixed with alumina powder by conventional ball-milling. In addition, in the regions where many CNFs were distributed, the CNFs migrated with the alumina grain boundaries during grain growth of alumina and then formed bundles. Such non-uniform mixing and formation of CNF bundles were remarkable for the 5.0 wt% CNF/alumina composites.

The average alumina grain sizes and alumina grain size distributions of the 0.4–5.0 wt% CNF/alumina composites are shown in **Figs. 5** and **6**, respectively. While the average alumina grain size of the 0.4 and 0.8 wt% CNF/alumina composites increased rapidly with an increase in sintering temperature from 1375 to 1450°C, that of the 1.6–5.0 wt% CNF/alumina composites increased gradually with an increase in sintering temperature from 1375 to 1525°C. As the addition of CNFs increased from 0.4 to 1.6 wt%, the alumina grains with a size of more than 3 μm decreased and the grain size distribution became narrower, as shown in Fig. 6. In the 1.6 wt% CNF/alumina composite, the size of the alumina grains was below 3 μm. On the other side, the grain size distribution of the 2.5 wt% CNF/alumina composite extended to a larger grain size side compared with that of the 1.6 wt% CNF/alumina composite, and that of the 5.0 wt% CNF/alumina composite was almost the same as that of the 1.6 wt% CNF/alumina composite. Actually, in the 5.0 wt% CNF/alumina composites, large alumina grains with 5–10 μm existed in the regions where a few CNFs were distributed as

shown in Fig. 3(f); however, such large grains were not caught in the measurement of alumina grain size because there were only a few such regions.

On the other hand, the 0.4 wt% CNF/alumina composite sintered by PAS had a larger average alumina grain size than the 0.4 wt% CNF/alumina composite sintered in vacuum and then treated by HIP; notably, the composites sintered by PAS at 1450°C, as shown in Fig. 5(b). That is, the unique sintering process of PAS accelerated the alumina grain boundary migration rate during sintering and the addition of 0.4 wt% CNFs was not enough to retard the rapid grain boundary migrations during PAS. Consequently, 14, 17 and 20% of CNFs entered alumina grains during PAS at 1300, 1375 and 1450°C, respectively, and alumina grains grew rapidly at 1450°C, which was different behavior from the composite sintered in vacuum and then treated by HIP.[17] The grain growth behavior of the 0.8 wt% CNF/alumina composites was similar to that of the 0.4 wt% CNF/alumina composites.

In the 1.6 wt% CNF/alumina composites in which 60% of CNFs distributed as solo, because not only solo CNFs but also CNF bundles distributed uniformly at grain boundaries of alumina, the rapid alumina grain boundary migrations during PAS was effectively retarded by such CNFs. Consequently, the 1.6 wt% CNF/alumina composites had a smaller average alumina grain size with a narrower grain size distribution. In the 2.5 and 5.0 wt% CNF/alumina composites sintered at 1375°C, half of the CNFs and three-quarters of the CNFs formed bundles, respectively. The formed CNFs bundles made the grain growth retardation effect of the CNFs lower in these composites. Consequently, the average alumina grain size of the 2.5 wt% CNF/alumina composite was almost the same as that of the 1.6 wt% CNF/alumina composite and that of the 5.0 wt% CNF/alumina composite was slightly smaller than that of the 1.6 wt% CNF/alumina composite, though the alumina grain sizes of CNT/alumina composites generally decrease with an increase in the amount of CNTs.[11),13),14),25)]

3.3 Fracture toughness

The fracture toughness of the 0.4–5.0 wt% CNF/alumina composites sintered by PAS at 1300–1525°C for 80 s are shown in **Fig. 7**. In this study, the fracture toughness of the 1.6 wt% CNF/alumina composite sintered at 1300°C for 80 s was the highest (5.4 MPa·m$^{0.5}$), which was 54% higher than that of monolithic alumina (3.5 MPa·m$^{0.5}$). The fracture toughness of the composites increased with an increase in CNF content from 0 to 1.6 wt%, showed a maximum at 1.6 wt% and decreased with an increase in CNF content from 1.6 to 5.0 wt%. SEM images of Vickers cracks of the 0.4–5.0 wt% CNF/alumina composites sintered at 1375°C for 80 s are shown in **Fig. 8**. Almost Vickers cracks on the CNFs/alumina composites were not deflected, but bridging and/or pull-out of CNFs were observed in the cracks, which means that the enhancement of the fracture toughness of the composites resulted from the bridging and/or pull-out of CNFs.

The relationship between fracture toughness and the average alumina grain size of the CNF/alumina composites is shown in **Fig. 9**. The fracture toughness of the composites tended to increase with a decrease in the average alumina grain size. The solid line in Fig. 9 is the curve for the relationship between fracture toughness and average alumina grain size of the 0.4 wt% AT05-CNF/alumina composites sintered in vacuum and then treated by HIP, which was shown in our previous study.[17] The fracture toughness of the 0.4–2.5 wt% CNF/alumina composites were mostly fitted to the curve but those of the 5.0 wt% CNF/alumina composite obviously deviated from the curve as indicated by a dotted circle in Fig. 9. The fracture toughness of the 5.0 wt% CNF/alumina composite were lower than those of the 1.6 and 2.5 wt% CNF/alumina composites even at the same average alumina grain size, which resulted from the formation of more CNF bundles in the 5.0 wt% CNF/alumina composite. That is, the number of CNFs giving rise to the essential effect for bridging and/or pull-out was distinctly reduced in the 5.0 wt% CNF/alumina composite in which three-quarters the number of CNFs formed bundles. Consequently, the fracture toughness of the 5.0 wt% CNF/alumina composite deviated from the curve.

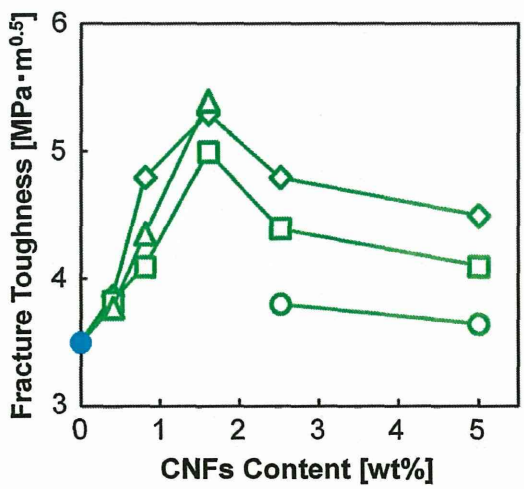

Fig. 7. Fracture toughness of the 0.4–5.0 wt% CNF/alumina composites sintered by PAS at (△) 1300°C, (◇) 1375°C, (□) 1450°C and (○) 1525°C for 80 s, and that of (●) monolithic alumina sintered in air at 1300°C for 2 h and then treated by HIP.

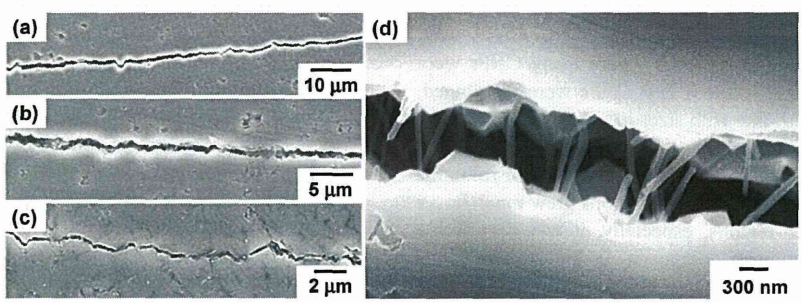

Fig. 8. SEM images of Vickers cracks on the (a) 0.4, (b,d) 1.6 and (c) 5.0 wt% CNF/alumina composites sintered by PAS at 1375°C for 80 s.